

Development of a High-Speed VUV Camera System for 2-Dimensional Imaging of Edge Turbulent Structure in the LHD

Masaki TAKEUCHI, Satoshi OHDACHI and LHD experimental group

National Institute for Fusion Science, 322-6 Oroshi-cho, Toki 509-5292, Japan

(Received 9 January 2009 / Accepted 15 August 2009)

To clarify the role of edge turbulent transport, measurements of fluctuations with high temporal and spatial resolution are necessary. In this case, if 2-dimensional structures are observed, more detailed characteristics of edge turbulence can be clarified, since the propagation direction of the fluctuations and the mode number are directly visually studied. Therefore, a high-speed vacuum ultraviolet (VUV) camera system for 2-dimensional imaging of edge turbulent structures was developed and installed in the Large Helical Device (LHD). This optical system is composed of two multi-layer mirrors made of Mo/Si and a micro-channel plate (MCP). VUV emissions from plasmas are reflected at the multi-layer mirrors with high reflectivity and imaged on the MCP. The VUV emission of impurity carbon ($n = 4-2$ transition of C VI) near 13.5 nm can be observed with this system. In this paper, the components of this VUV camera system and the analytical method and calculations are described in detail. Moreover, preliminary results observed in the LHD are presented.

© 2010 The Japan Society of Plasma Science and Nuclear Fusion Research

Keywords: 2-dimensional imaging, vacuum ultraviolet, impurity carbon, turbulent structure

DOI: 10.1585/pfr.5.S1037

1. Introduction

In fusion plasmas, edge turbulent transport greatly affects plasma confinement. For plasmas with an edge transport barrier, edge turbulence suppression by sheared $E \times B$ flow has been observed [1]. Recently, oscillating $E \times B$ flows called zonal flows have emerged as an important part of the overall physics of turbulence [2].

The measurement of edge turbulence requires both high temporal and high spatial resolution. A 2-dimensional edge turbulent structure is necessary to clarify the propagation direction of fluctuations, mode structure, and so on. In the Large Helical Device (LHD), an edge transport barrier and an internal diffusion barrier have recently been observed and intensively studied. Measuring the edge turbulent structure in the plasmas is important for clarifying the physical mechanisms of these transport barriers.

Therefore, we have developed a new 2-dimensional imaging diagnostic for edge turbulent structures, the high-speed vacuum ultraviolet (VUV) camera system. VUV emission from impurity carbon reflects a density fluctuation, from which the edge density fluctuation can be estimated. This system is more sensitive than a pinhole-type optical system. This high-speed VUV camera system was installed on the LHD, and preliminary data were obtained.

2. High-speed VUV camera system

A high-speed VUV camera system consists of multi-layer mirrors, a micro-channel plate (MCP), and a visible high-speed camera, as shown in Fig. 1 (a). Since VUV

light is transferred only in a vacuum region, the whole system is placed in a vacuum chamber except for the visible high-speed camera.

The multi-layer mirrors are made of Mo/Si (typical thickness: 6.66 nm, $d_{\text{Mo}}:d_{\text{Si}} = 4:6$) and the reflectivity is about 50–60% [3]. These mirrors reflect mainly VUV light of 13.5 nm (half-band width: about 1–2 nm). This wavelength corresponds to the impurity carbon line ($n = 4-2$ transition of C VI) [4]. The system has two multi-layer mirrors. One reflects the VUV light by a convex mirror (curvature radius: 144.5 mm); the other reflects the light and images onto a detector by a concave mirror (curvature radius: 390 mm), as shown in Fig. 1 (a). The diameter of the first mirror is 23.2 mm. The number of photons collected by this mirror is much larger than that measured by a simple pinhole camera.

An MCP (Burle Industries Inc., APD 3040FM 12/10/8 I 60:1 P-20), which can multiply secondary electrons 2-dimensionally, is used for detection. Particles, VUV light, and X-ray light can produce secondary electrons. Therefore, an MCP is generally used to detect them. In the high-speed VUV camera system, the multi-layer mirrors do not reflect X-ray light, and charged particles do not come to the MCP due to the magnetic field in the LHD. Neutral particles do not directly enter the MCP because the multi-layer mirrors block the direct path to the MCP. The effect of the entrance of scattered neutral particles is considered to be small. Moreover, the MCP is negatively biased in order to repel secondary electrons generated in the VUV camera system. Thus, it is mainly VUV light of 13.5 nm

author's e-mail: m-takeuchi@nifs.ac.jp

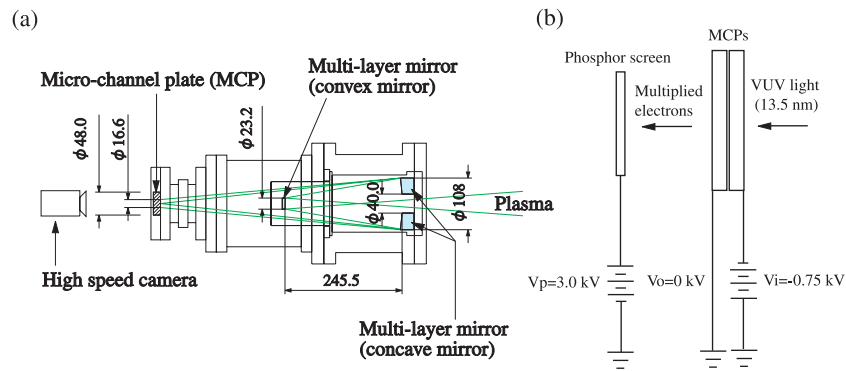


Fig. 1 (a) High-speed VUV camera system and (b) micro-channel plate section.

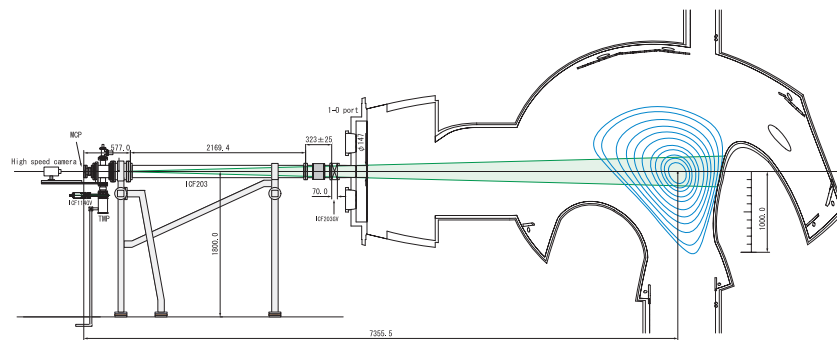


Fig. 2 Comprehensive view of high-speed VUV camera system together with LHD vacuum vessel and plasma.

that is multiplied by the MCP, and we can use the MCP as a VUV detector. The MCP has two layers; high voltages are supplied to them as shown in Fig. 1 (b). One, on the plasma side, is the input (V_i); the other, on the phosphor side, is the output (V_o). Typical applied V_i and V_o voltages are -0.75 kV and 0 V, respectively. The MCP used here has a phosphor screen 48 mm in diameter to image the output signal optically. For the phosphor, voltage is supplied up to $V_p = +3.0$ kV to project multiplied electrons to the phosphor screen.

The intensity of the radiation from the plasma varies significantly as the plasma parameters change. Therefore, the multiplication factor at the MCP should be carefully controlled; we remotely control the high-voltage power supply to adjust the multiplication factor.

The 2-dimensional image on the phosphor screen is recorded by a visible high-speed camera. We use a Phantom v4.2 camera made by Vision Research, Inc. which can record up to $25,400$ pictures per second (pps) at 128×128 pixels; data from this camera are digitally recorded in 8 bits. The obtained data are transferred to a PC through an optical fiber and stored on the PC.

A comprehensive view of the high-speed VUV camera system together with the LHD vacuum vessel and plasma is shown in Fig. 2. The focal length of the multi-layer mirrors is about 7 m; thus, the mirrors are displaced from the plasma center by this length. The plasma image is re-

duced to $1/60$ by the mirror optics and focused on the MCP screen. Since the diameter of the diagnostic port used here is smaller than that in the initial design, only $1/3$ of the image, which corresponds to 5.5 mm at the entrance of the MCP, can be measured at present.

3. Viewing area and simulated image

A top view of the magnetic field lines and viewing area of the VUV camera are shown in Fig. 3 (a). Figure 3 (b) shows the last closed flux surface at poloidal planes projected onto the MCP screen. In this viewing field, only the area indicated by the blue circle can be measured, due to the limited diagnostic port size. The magnetic field lines in the horizontally elongated section at $R_{ax} = 3.8$ m, $B_{ax} = -2.763$ T, and $\gamma = 1.262$ are shown in Fig. 4. The plasma is surrounded by the ergodic region. It is possible to measure the C VI radiation from this ergodic layer together with the plasma. The trace of the X-points in Fig. 4 is shown in Fig. 3 (b) by green Xes.

At this viewing angle, if the radiation is exactly localized on a flux surface, we can measure the 2-dimensional images of the fluctuations. However, the radiation area might be thicker. We would then need to reconstruct the local emissivity from line-integrated data. To reconstruct the structure, we must assume that the radiation along the magnetic field lines is constant. Then, each point on the sight-

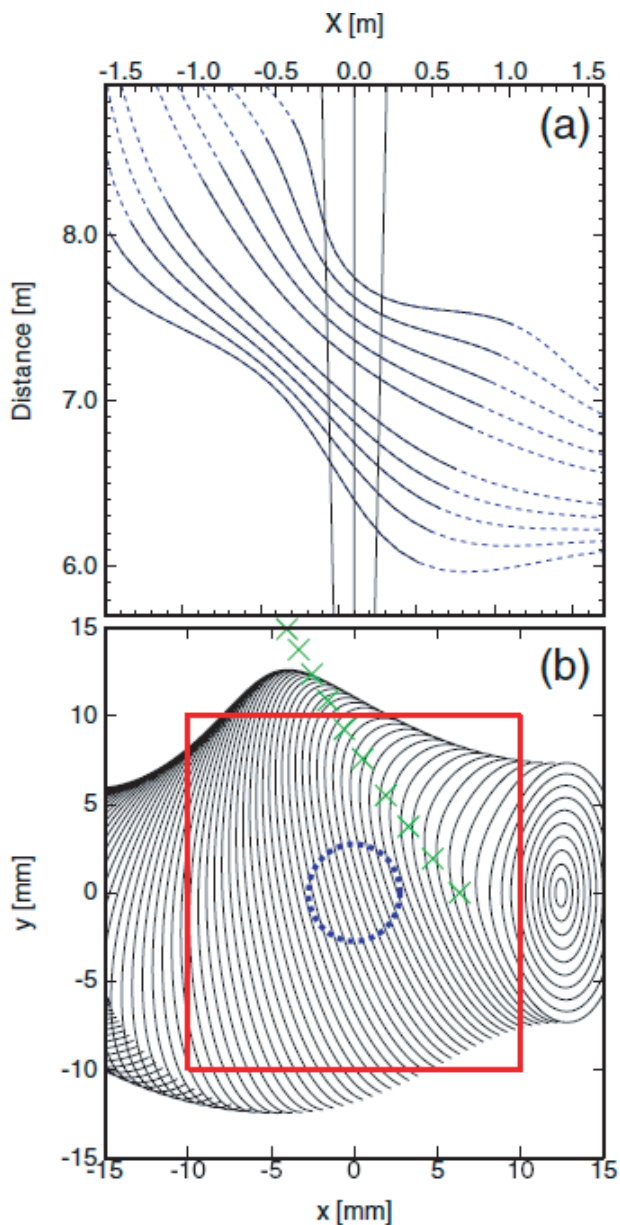


Fig. 3 (a) Top view of magnetic field lines and sight lines of VUV camera. Vertical axis shows the distance from the MCP. (b) Last closed flux surfaces [solid line area in (a)] projected onto MCP detector plane. The x and y axes are coordinates on the MCP. Blue circle represents the area where signal is expected. Green Xes are the X-points of magnetic field lines in Fig. 4. Red quadrangle corresponds to the region used in Fig. 5.

lines can be converted to a point on a reference flux surface. We can simulate the line-integrated image by assuming the local emissivity on the reference flux surface [5–7].

Figure 5 shows a simulated image of the VUV camera using the method described above. In the calculation, the radiation profile is assumed to be proportional to $\exp(-((\rho - 0.7)/0.1)^2)$. Here, ρ is the normalized minor radius. The peak of the radiation is determined by the location where the C^{5+} ions are localized. It is estimated

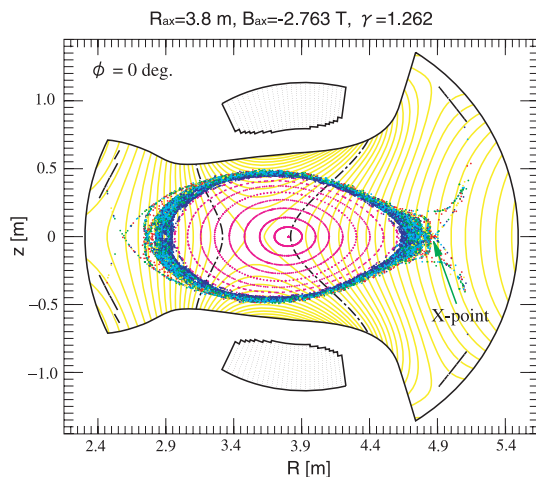


Fig. 4 Magnetic field lines in horizontally elongated section at $R_{ax} = 3.8$ m, $B_{ax} = -2.763$ T, and $\gamma = 1.262$.

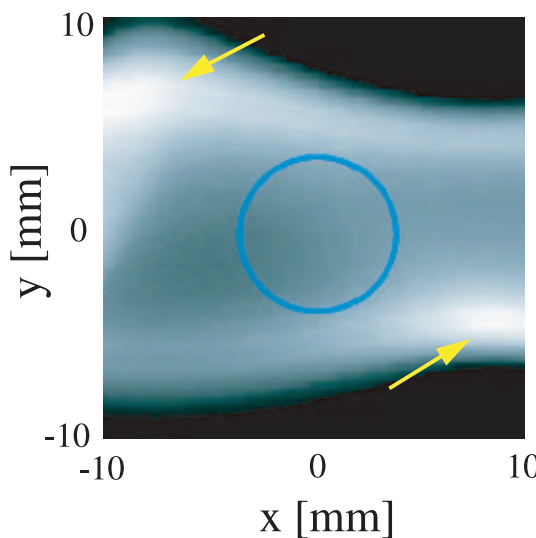


Fig. 5 Simulated image of VUV camera based on calculation. Image region corresponds to red quadrangular region in Fig. 3 (b), and blue circle represents the imaging area of the MCP.

by the IONEQ code [8] developed by Dr. A. Weller, using plasma parameters in the experimental condition shown in Fig. 7.

The upper-left and lower-right areas indicated by arrows are brighter than other areas. This is due to geometrical effects; the length of sightlines within the edge radiation region is longer for the two brighter areas (see Fig. 3). Also, in the viewing area denoted by the circle, the lower left area is darker than other areas. The latter characteristic can also be seen in the experimental data.

4. Experimental results

Preliminary data were obtained by the present system in the LHD. The following data were measured by the camera with a speed of 4000 pps and an area of 144×128 pixels.

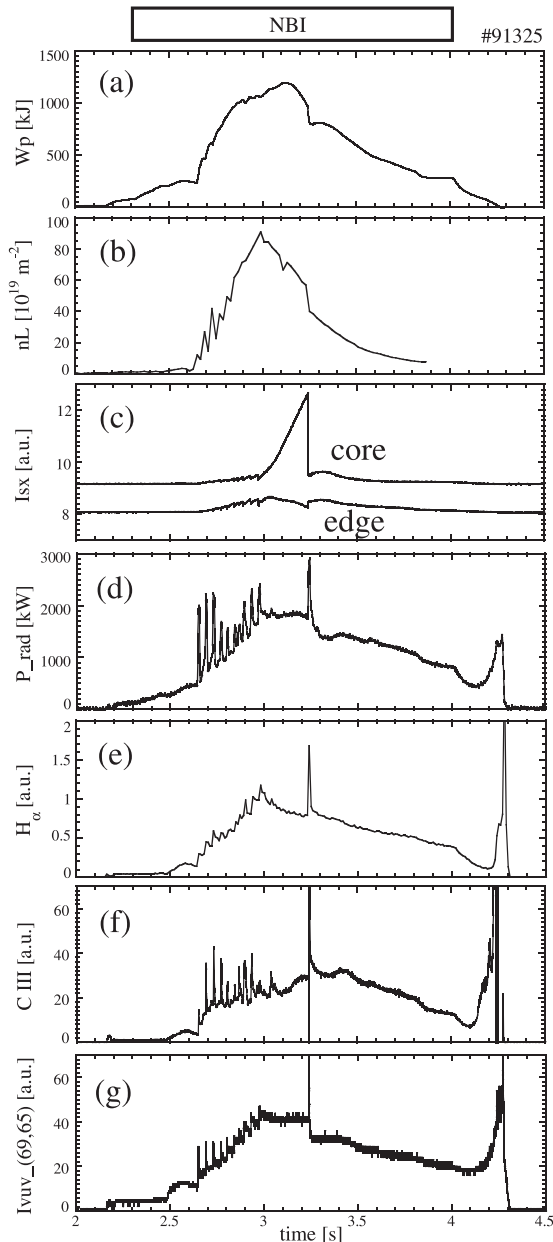


Fig. 6 Time evolution of NBI: (a) W_p , (b) nL , (c) I_{sx} , (d) P_{rad} , (e) H_α , (f) C III, and (g) VUV emission at $(x, y) = (69, 65)$ pixels, which is the center of the MCP. The CDC occurs at $t = 3.24$ s.

Figure 6 shows the time evolution of neutral beam injection (NBI), plasma stored energy (W_p), line-integrated electron density (nL), intensity of soft X-ray radiation (I_{sx}), total power of radiation (P_{rad}), H_α emission, C III emission, and measured VUV emission at $(x, y) = (69, 65)$ pixels, which is the center of the MCP. The plasma was heated by four NBIs, and hydrogen pellets were injected for $t = 2.65$ - 3.0 s. The electron density suddenly decreases at $t = 3.24$ s, as shown in the nL panel. The I_{sx} observed in the core plasma also rapidly decreases, and that in the edge plasma slightly increases. This event is called core density collapse (CDC) [9]. The radial profiles of T_e and n_e before

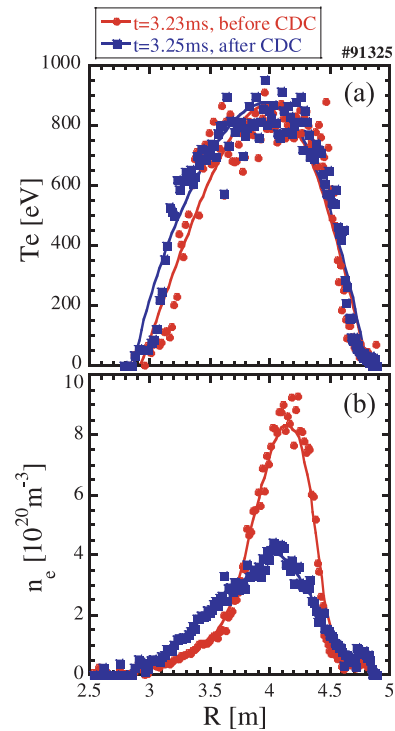


Fig. 7 Radial profiles of (a) T_e and (b) n_e before and after CDC from Thomson scattering measurements.

and after CDC from Thomson scattering measurements are shown in Fig. 7. The electron density in the core region decreases, and the density of the edge region increases. The time evolution of the emission at $(x, y) = (69, 65)$ is similar to that of C III emission, P_{rad} , and H_α emission. A rapid change at the CDC event is clearly detected in the present system. The ability to measure a 2-dimensional VUV image with a very fast framing rate is demonstrated here. However, the increase in the signal at the end of the discharge might be caused by low-energy stray light. Therefore, the observed signal might be not only carbon impurity emission at 13.5 nm. We will improve the high-speed VUV camera system by using a low-energy cut-off filter to prevent stray light. A Zr thin film is planned at present.

The 2-dimensional images just before the CDC at $t = 3.2375$ s and just after the CDC at $t = 3.23975$ s, $t = 3.24025$ s, and $t = 3.24175$ s are shown in Fig. 8. The emission outside the imaging area (> 5.5 mm) is stray light. As in the simulated image of Fig. 5, the lower area is darker than other regions. Just after the CDC in (b), two bright linear emission features are observed. From (b) to (d), the bright area quickly changes its shape. This might be caused by high-density plasma escaping from the core region during the CDC event. The angle of the linear emission is similar to the angle of the X-point in Fig. 3 (b), which may suggest plasma outflow toward the X-point. These changes in the 2-dimensional VUV emission indicate that the outflow of plasma density from the core to the

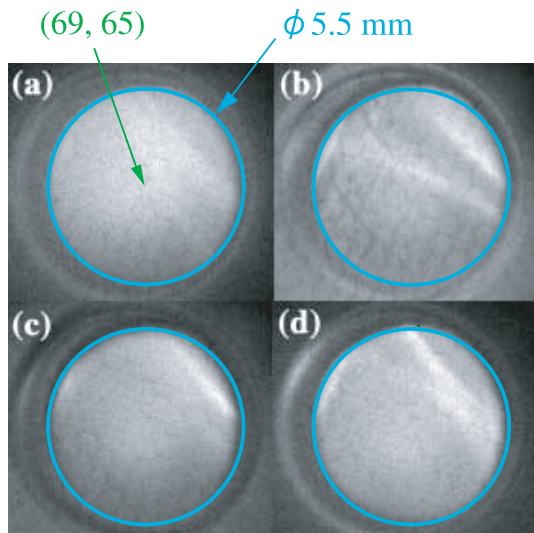


Fig. 8 2-dimensional images just before the CDC at $t = 3.2375$ s (a), and just after the CDC at $t = 3.23975$ s (b), $t = 3.24025$ s (c), and $t = 3.24175$ s (d). Region inside the circle 5.5 mm in diameter represents the imaging area of the MCP.

edge region is not spatially uniform. The reconstruction of this 2-dimensional VUV emission is now proceeding.

5. Summary

A high-speed VUV camera system was developed, and preliminary data were obtained. Two-dimensional VUV emissions were successfully observed. To observe

the edge turbulent structure, it is necessary to improve the present system to observe VUV emission at higher temporal resolution. It was demonstrated that the new diagnostic system can be a useful and powerful tool for imaging 2-dimensional edge turbulent structures in fusion plasmas.

Acknowledgments

This study was supported by NIFS budget code NIFS08ULHH509 and also partially by the Ministry of Education, Science, Sports and Culture, Grant-in-Aid for Scientific Research (B), 17360446, 2005-, the IAEA TEXTOR agreement (NIFS07KETE001), and the JSPS-CAS Core University Program in the field of Plasma and Nuclear Fusion.

We express our gratitude to Dr. Kuninori Sato for the loan of his MCP and to Dr. A. Weller for use of the IONEQ code.

- [1] P.W. Terry, *Rev. Mod. Phys.* **72**, 109 (2000).
- [2] P.H. Diamond *et al.*, *Plasma Phys. Control. Fusion* **47**, R35 (2005).
- [3] H. Takenaka *et al.*, *Transactions of MRS-Japan* **28**, 95 (2003).
- [4] D. Stutman *et al.*, *Rev. Sci. Instrum.* **77**, 10F330 (2006).
- [5] S. Ohdachi *et al.*, *Plasma Sci. & Tech.* **8**, 45 (2006).
- [6] Y. Nagayama, *J. Appl. Phys.* **62**, 2702 (1987).
- [7] N. Iwama and S. Ohdachi, *J. Plasma Fusion Res.* **82**, 399 (2006).
- [8] A. Weller *et al.*, *JET-IR(87)10*.
- [9] J. Miyazawa *et al.*, *Plasma Fusion Res.* **3**, S1047 (2008).